A Method for Health Indicator Evaluation for Condition Monitoring of Industrial Robot Gears

Corbinian Nentwich *[ID] **and Gunther Reinhart**

Institute for Machine Tools and Industrial Management, Boltzmannstraße 15, 85747 Garching, Germany;
emeritus.reinhart@tum.de
* Correspondence: corbinian.nentwich@iwb.tum.de

Abstract: Condition monitoring of industrial robots has the potential to decrease downtimes in highly automated production systems. In this context, we propose a new method to evaluate health indicators for this application and suggest a new health indicator (HI) based on vibration data measurements, Short-time Fourier transform and Z-scores. By executing the method, we find that the proposed health indicator can detect varying faults better, has lower temperature sensitivity and works better in instationary velocity regimes compared to several state-of-the-art HIs. A discussion of the validity of the results concludes our contribution.

Keywords: industrial robot; condition monitoring; health indicator

1. Introduction

Industrial robots are a fundamental part of highly automated production systems, which can be found in the automotive or electronics industry [1]. Since they operate in complex production cells and as a part of linear production lines, robot malfunctions lead to long downtimes for repair or replacement and, hence, to increased costs. In particular, robot gear faults are responsible for the longest downtimes because they often require the replacement of the whole robot [2]. The condition monitoring (CM) of these gears offers the potential to resolve this issue. CM is the monitoring of an asset's health using sensor data. The health state represents a wear reserve before a failure occurs. This health state is quantified with a health indicator (HI). A significant monitored change in this health indicator can be used as a decision-making aid in the planning of maintenance actions [3].

1.1. State-of-the-Art

In recent years, different HIs based on vibration data for several industrial robot components, such as bearings, gears and motors, and their specific faults have been investigated. Furthermore, several approaches to cope with instationary signals in CM have been presented. The next two sections give a short overview of these topics followed by a section stating the contribution of our publication.

1.1.1. Vibration-Based Robot Condition Monitoring

A fault detection method was developed in [4], which first uses a novel phase-based, time-domain averaging method to remove the deterministic part of the vibration signal. Subsequently, the root mean square (RMS) and power spectrum entropy of the remaining residual signal are calculated as health indicators. A vibration signal based CM system for SCARA robots was implemented in [5], which in the first step uses statistical HIs of the time-domain signal to detect the occurrence of a defect and in the second step uses an artificial neural network to diagnose the fault type. A three-layer architecture for remote fault diagnosis of industrial robot gearboxes was proposed using vibration signals in [6]. In the diagnosis layer, the authors present a performance evaluation approach using a support vector machine (SVM), a remaining useful life prediction by a Markov

model and a fault-type diagnosis based on a Bayesian network. The degenerative behavior of an industrial robot gear was observed with vibration sensors by [7] as well as [8] in accelerated wear tests. After pre-processing the signals using order tracking and spectral auto-correlation, the characteristic fault frequencies were calculated and monitored by root mean square analysis, which revealed a trend correlating with increasing wear. In addition to the installation of accelerometers, other additional data sources were investigated in this context. The acoustic emission technology was used to detect robot gearbox faults based on the ball spinning and ball passing frequency of the bearings in [9]. The changes of the RMS-HI and characteristic frequencies for functional and broken strain gears of industrial robots were investigated in [10]. The classification and regression performance of different data-driven models based on frequency-domain data and principal component analysis for dimensionality reduction was evaluated in [11].

1.1.2. Time–Frequency-Based Health Indicators

In addition to vibration data based CM approaches for industrial robots, there also exist several publications considering HIs from the time–frequency-domain. Here, approaches based on the Short-time Fourier transform (STFT), Wavelet transform (WT) or Hilbert Huang transform (HHT) can be divided. STFT is used to derive two HIs named Prominence and Compliance in [12] to detect bearing faults based on their characteristic fault frequencies. A similarity measure between the STFT spectrograms based on standard deviation and correlation is combined with a simple classifier in [13] to detect bearing faults. The same objective was pursued in [14] by means of the marginal time integration of STFTs. Bearing fault classification by means of non-negative matrix factorization or convolutional neural networks and STFT was evaluated in [15,16].

In the field of WT, several approaches exist for different assets. CM of brushless DC motors is investigated based on energies for characteristic frequencies based on both STFT and WT in [17]. A decomposition rate is used in [18] for CM of electric drives based on WT. RMS and Kurtosis are calculated for the WT coefficients for broken bar fault detection in electric drives and combined with a neural network for fault classification in [19]. Bearing fault classification was performed with an SVM based on WT in combination with singular value decomposition for dimensionality reduction in [20]. The spectra of WT coefficients were the basis for the calculation of statistical HIs and frequency specific energy values for the CM of bearing faults in [21]. The similarities of continuous WT spectra are used as an HI for bearing fault detection [22]. The permutation entropy derived from flexible analytical wavelet transform was used as a feature for an SVM for bearing fault classification [23]. Impulse factor, Kurtosis and RMS based on WT coefficients were used for bearing fault detection of helicopters [24]. Statistical features and Hoelder's exponent were derived from WT coefficients for milling tool health state monitoring. Here, the HIs were the input for an SVM and Decision Tree classifier [25]. HIs were derived by a convolutional neural network for milling tool condition monitoring based on the wavelet decomposition in [26]. Energies of WT coefficients were also used for detecting generator and gear faults in wind turbines [27]. Different entropy-based and statistical features were used in [28] for gearbox health monitoring in combination with an SVM. Energy and entropy values derived from WT for characteristic frequencies are applied for gearbox condition monitoring in [29].

In [30], the Shannon entropy based on HHT was used for the CM of gears. HHT was also used in [31] to derive HIs by an autoencoder based on the Marginal Hilbert Spectrum. A component dependent frequency energy based on HHT was used as a label in [32] for a CNN-based regression model trained on raw vibration time series data for bearing fault detection. Different statistical and entropy-based HIs were calculated from the Intrinsic mode functions (IMFs) derived by HHT in [33].

1.2. Contribution to the State-of-the-Art

However, none of these publications assess vibration data-based HIs' ability to detect faults in an industry-like industrial robot application setting. It is characterized by

changing robot axes' velocities, changing temperatures of the gears due to unbalanced robot utilization and unknown robot gear fault types. This is why we present a new HI for robot gear condition monitoring, which potentially copes with these characteristics. Furthermore, we propose a method to evaluate the suitability of HIs for the task of robot gear condition monitoring. We apply this method on the newly formulated HI and several HIs from the state-of-the-art.

2. Materials and Methods

This section is divided in two parts. First, the newly developed HI is presented. Afterwards, the methodologies to evaluate the HI's performance and data sets used in this context are explained.

2.1. Time–Frequency-Domain-Based Z-Score

The concept of the newly designed HI is based on two cornerstones. To deal with instationary velocity regimes, which are found in robot applications due to the typical movement patterns of a robot, the HI is based on time–frequency-domain data. Simultaneously, the HI must take into account a certain variance of this data due to environmental changes such as temperature fluctuations. This is realized by the concept of Z-scores, a common similarity measure from statistics [34]. The process to calculate the new HI is depicted in Figure 1.
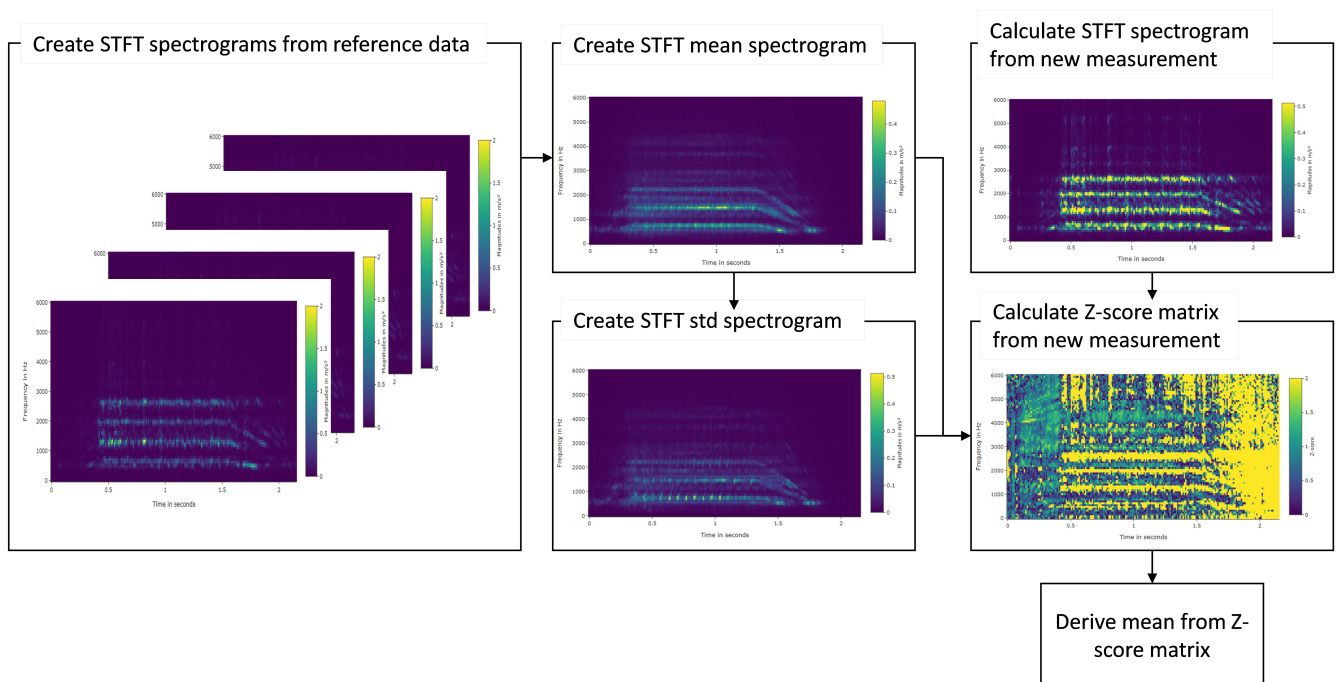

Figure 1. Process to derive the Z-score-based HI.

In detail, the new HI is based on high-frequency sampled acceleration sensor data. Data from one measurement are transformed to a time–frequency-spectrogram by usage of the STFT, which is calculated according to Equation (1). Here, τ and ω are time and frequency indices, $x(n)$ is the time series signal of the vibration signal at timestep n and w is a windowing function with the length R.

$$spec(\tau, \omega) = \left| \sum_{n=-\infty}^{\infty} x(n)w(n - \tau R)e^{-j\omega n} \right| \tag{1}$$

To set up the HI, a certain number of vibration signal spectrograms must be collected for the robot to capture its signal signature in a healthy state with its stochastic variations.

This takes place in an initialization phase. For this, initially, two measurements must be collected. In this context, a measurement is defined as the collection of vibration data over one single movement. Based on this data, the two spectrograms are calculated. To determine whether this reference quantity of two spectrograms captures the stochastic variation of the signal, the overall mean (Equation (2)) and standard deviation (Equation (3)) of the spectrograms are calculated.

$$spec(\tau, \omega)_{avg} = \frac{1}{k} \sum_{i=0}^{k} spec(\tau, \omega)_i \tag{2}$$

$$std_{spec, \, overall} = \frac{1}{0.5FT} \sum_{\tau=0}^{T} \sum_{\omega=0}^{0.5F} \sqrt{\frac{\sum_{i=0}^{k}(spec(\tau, \omega)_i - spec(\tau, \omega)_{avg})^2}{k}} \tag{3}$$

In these formulas, k describes the number of measurements in the reference quantity. T is the time length of each measurement, F is the sampling frequency and $spec(\tau, \omega)_{avg}$ is the average value of $spec(\tau, \omega)$ over measurements 0 to k. Afterwards, one measurement is added to the reference quantity at a time, and again $avg_{spec,overall}$ and $std_{spec,overall}$ are calculated. Plotting these standard deviations over the number of measurements in the reference quantity usually first shows an increase in $std_{spec,overall}$ and then a saturation as can be seen in Figure 2. If this saturation is reached, the reference quantity can sufficiently represent the stochastic behavior of the signal signature. In the shown example, this saturation is reached after 5 measurements.
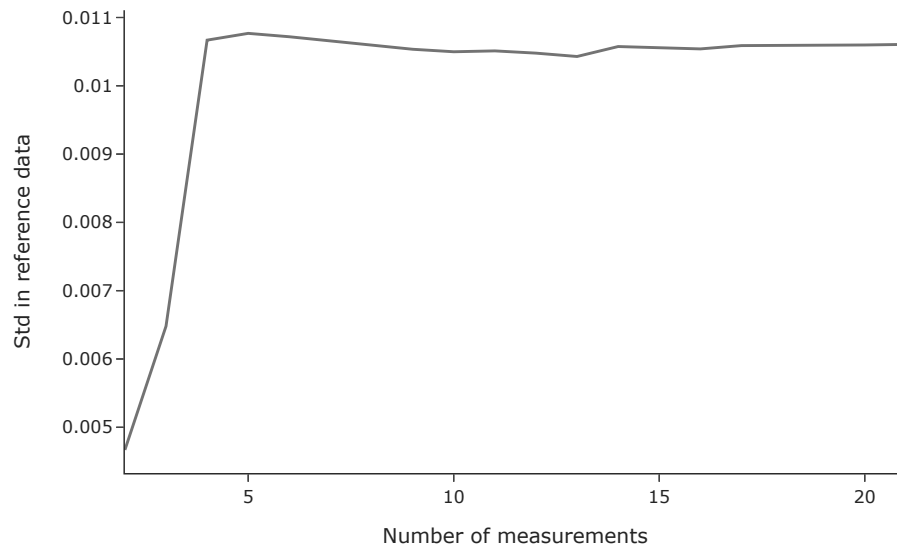

Figure 2. Saturation of the standard deviation in the time–frequency spectrograms.

After the initialization, an HI can be determined based on a newly collected measurement. For this, the measurement's spectrogram overall Z-score is determined according to Equation (4) .

$$HI_{meas} = \frac{1}{0.5FT} \sum_{\tau=0}^{T} \sum_{\omega=0}^{0.5F} \left| \frac{spec(\tau, \omega)_{meas} - spec(\tau, \omega)_{avg,ref}}{spec(\tau, \omega)_{std,ref}} \right| \tag{4}$$

In this context, $spec(\tau, \omega)_{avg,ref}$ and $spec(\tau, \omega)_{std,ref}$ are the mean value and the standard deviation of $spec(\tau, \omega)$ for all measurements in the reference quantity. In Figure 3, the STFT and Z-score spectrograms of exemplary vibration measurements from a healthy and a faulty robot gear are depicted. The Z-score-based spectrogram of the faulty measurement shows more prominent changes compared to the STFT-based spectrogram.
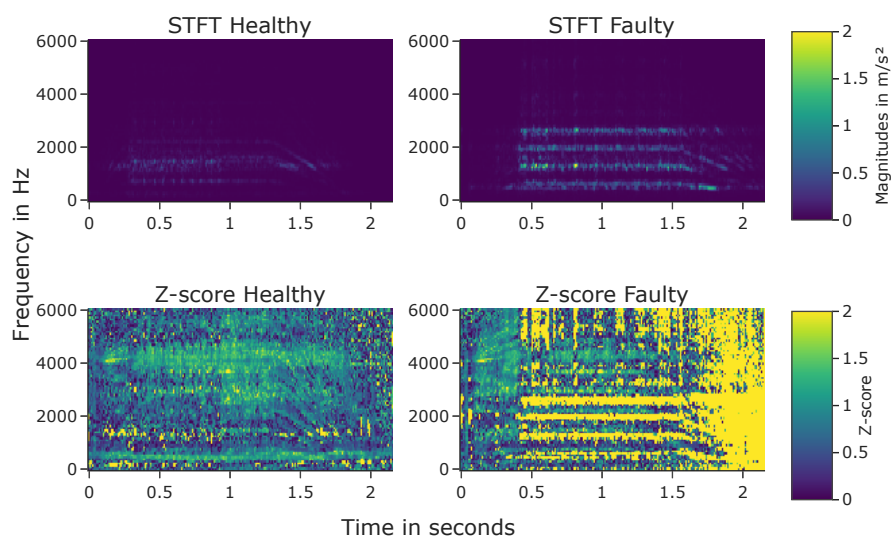
Figure 3. Comparison of STFT and Z-score spectrograms from healthy and faulty robot gear measurements.

2.2. Hi Evaluation Method

To compare the ability of the newly designed HI to cope with industrial robot application characteristics, we followed a three step approach. First of all, we investigated how well the designed HI can detect different kinds of faults in comparison to HIs from the state-of-the-art. Second, we investigated the temperature sensitivity of HIs from the state-of-the-art meeting this criterion and our HI. Third, we investigated the trend behavior of HIs showing a low temperature sensitivity on data from two accelerated wear tests. These three steps are now described more precisely. The overall process of our investigations is also described in Figure 4.
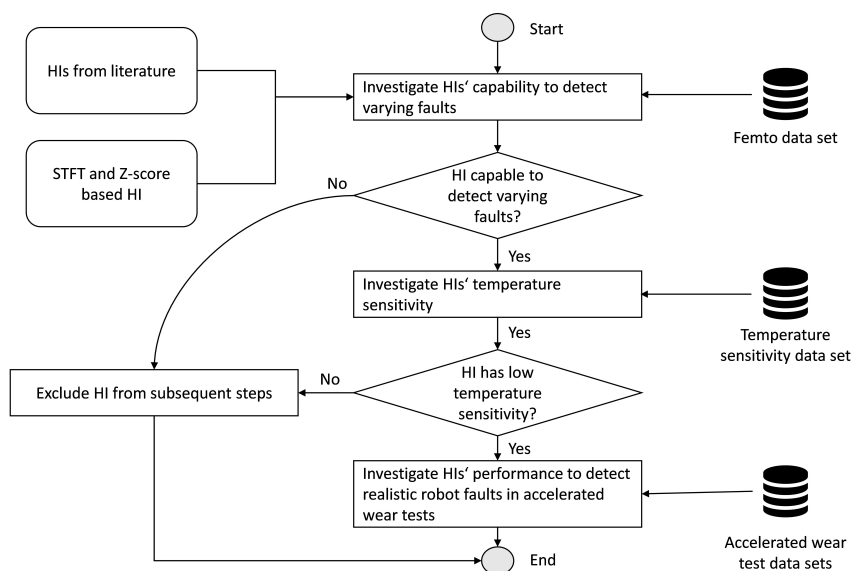
Figure 4. Overall process of the evaluation method.

2.2.1. Varying Fault Detection Analysis

We used the FEMTO data set, which is described in detail in [35], to select HIs capable of detecting different faults. The data set is available in [36]. This data set provides run to failure vibration data from 16 identical bearings and for different faults and working conditions defined by the applied load and the rotational speed. The acceleration sensor sampled data with 25.6 kHz, one measurement has a length of 0.1 s and measurements were

taken in equidistant timesteps of 10 s for all bearings. The test run for one bearing ended when the signal from the acceleration sensor exceeded 20 g. Therefore, different numbers of measurements are available per bearing ranging from 230 to 2803. We calculated the HIs summarized in Table 1 for all measurements of one sensor. These HIs were derived from several review papers regarding gearbox and bearing CM [37–40] and the publications mentioned in Section 1. Therefore, the HI calculation was based either on the raw acceleration signal, an enveloped signal as described in [41] or the residual signal as suggested by [4]. Additionally, the newly designed HI presented in Section 2 was calculated for the measurements based on the raw signals.

Table 1. Calculated HIs.

HI Name	HI Abbreviation	HI Source
Crest Factor	CrF	[40]
Dominant Frequency	DomF	[37]
Impulse Factor	ImpF	[38]
Kurtosis	Kurt	[39]
Margin Factor	MarF	[38]
Mean	Mean	[40]
Median	Med	[40]
Median Frequency	MedF	[37]
Peak	Peak	[39]
Peak to Peak	PtP	[39]
Root Mean Square	RMS	[39]
Skewness	Skew	[40]
Spectral Centroid	SpC	[37]
Spectral Flux	SpF	[37]
Spectral Rollover	SpRO	[37]
Spectral Entropy	SpE	[4]
Standard Deviation	Std	[39]
Discrete Wavelet RMS	DWTRMS	[19]
Discrete Wavelet Impulse Factor	DWTImpF	[19]
Discrete Wavelet Kurtosis	DWTKurt	[19,38]
Discrete Wavelet Entropy	DWTEntr	[4,19]
Discrete Wavelet Decomposition Rate	DecompRate	[18]
Hilbert Huang Entropy	HHTEntr	[30]
Intrinsic Mode Function RMS	IMFRMS	[33]
Intrinsice Mode Function Impulse Factor	IMFImpF	[33]
Intrinsic Mode Function Kurtosis	IMFKurt	[33]
Intrinsic Mode Function Entropy	IMFEntr	[33]
Time Domain Integral	TDI	[14]
Z-score	Z-score	-

To detect whether these HIs are sensitive to multiple faults, different techniques can be applied. In addition to filter techniques, ensemble, wrapper and embedded methods exist [42]. However, the latter three techniques combine classification or regression models with HIs for their evaluation. Hence, this evaluation is always dependent on the used models. Thus, we chose to use filter methods for the evaluation. Here, different figures of merit for regression and classification tasks can be applied, such as trendability, robustness, monotony or discriminance [42]. To combine these different performance indicators, we fitted different basic functions on the HIs calculated for the last 20 percent of measurements per bearing. These functions were first and second degree polynoms, exponential and sigmoid functions. For each of the fits, we calculated the R^2 value. This means that we received four R^2 values per HI and bearing. High R^2 values of these fits correlate with a high trendability, monotony, robustness and discriminance, which are desirable for HIs. To evaluate whether an HI can detect several damages, we considered only the best R^2 value

per HI and bearing. We plotted the statistics of these 16 remaining R² values per HI as a boxplot. Suitable HIs should show high R² values with low variance.

2.2.2. Temperature Sensitivity Analysis

HIs showing this behavior were analyzed regarding their temperature sensitivity. For this purpose, we acquired vibration data from an industrial robot test rig. This test rig consists of a KUKA KR510 industrial robot with an attached load of 365 kg. We attached acceleration sensors close to the gearboxes as shown in Figure 5 on the right side. These sensors have a sampling rate of 26 kHz. The acceleration direction of the sensors was orthogonal to their contact area. For data acquisition, the robot performed a trajectory where each joint was moved individually at different speeds in an angle area of 10°, as described in Figure 6, and for different gear temperatures in the range of 25 °C and 60 °C and 5 °C steps. One measurement per axis lasted 8 s. The gear temperature was measured at the gearbox cap with an infrared thermometer. For each temperature step, four measurements were made. For each measurement at each temperature step, the remaining HIs were calculated. To determine the temperature sensitivity, we divided the average HI values calculated from measurements at the highest gear temperatures by the values calculated from measurements at the lowest temperature. HIs with a high sensitivity were eliminated for the last step.

ABB IR 7600 test bed　　　　　　　　　　　　　　KUKA KR 510 test bed
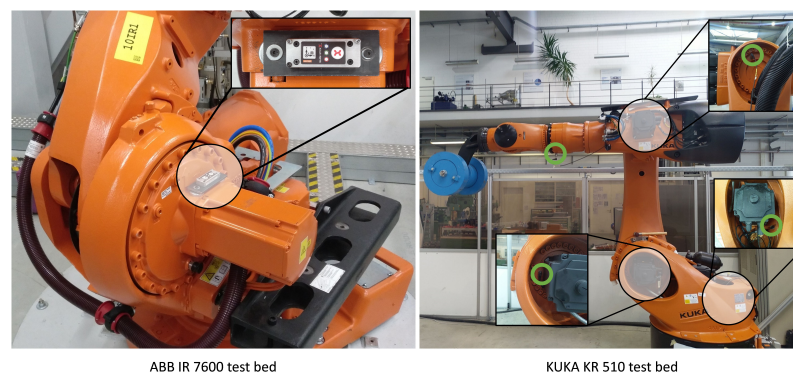
Figure 5. Robot test beds.
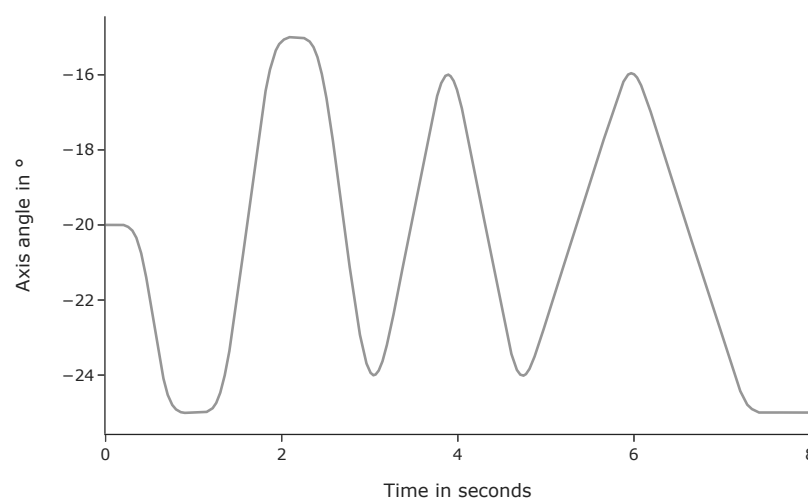
Figure 6. Measurement trajectory for the temperature sensitivity analysis.

2.2.3. Accelerated Wear Test Analysis

Here, we calculated the remaining HIs for measurements from two data sets from accelerated robot wear tests to see how these HIs perform in a more industry like setting

and how they cope with instationary velocity behavior. The first data set was collected during a time range of approximately one year with an ABB robot of type RB 6600-255/2.55. During the data acquisition, the robot performed an isolated movement of the second axis in an angle area of 150° for each measurement. Vibration data were only acquired with a sensor attached axially at the robot axis 2 gearbox. At the end of the experiment, the gearbox was dismantled and faults on the bearings and the shafts of the gear were found. A total of 2290 measurements, equally distributed over time, were taken for our analysis from this data set. One measurement lasted 1.6 s and the sampling rate was 10 kHz. More detailed information about this experiment can be found in [7,8]. The second data set was derived from another experiment. Here, the second axis of an ABB IRB 7600-340/2.8 was moved in an angle area of 80° continuously over the time frame of three months. The vibration sensor attached to the gearbox cap of axis 2 sampled with 20 kHz and one measurement lasted 2.15 s. The measurement setup is presented on the left side in Figure 5. The experiment ended after a roller element of a bearing had cracked and had blocked the gear. In this time range, 920 vibration measurements were taken in total in equidistant time steps. The faults, which occurred in both experiments, can be seen in Figure 7. In both experiments, environmental conditions such as load and trajectory were kept constant. Fluctuations of the temperature were kept at a minimum due to the constant movements of the robots. In this way, signal changes are likely to be correlated to increasing wear.

Faults of the IR 7600 experiment
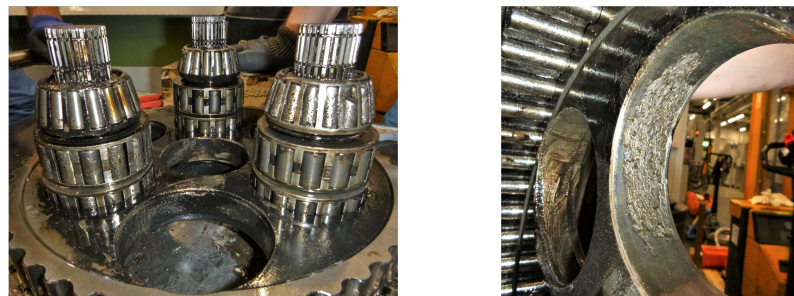
Faults of the IR 6640 experiment

Figure 7. Faults in the accelerated wear tests, lower image following [7].

3. Results

This section is divided in three parts. First, the results from the varying fault detection experiments are shown. Secondly, the results from the temperature sensitivity analysis are presented. Finally, the application of the HIs on the two accelerated wear tests is described.

3.1. Varying Fault Detection Analysis

From the 16 bearing experiments, the HIs presented in Table 1 were calculated. We used the first 100 measurements per bearing as the reference quantity for the Z-score-HI and set R to 128. Figure 8 shows the R² values for a selection of different HIs as a box plot. The R² statistics for all HIs can be found in Appendix A. The abbreviations of the HIs are explained in Table 1. The PtP-, Peak-, RMS-, Std- and Z-score-HI show the highest R² values on average. They also show the lowest variance between the different bearings. This means that these HIs detect different faults most reliably. Other HIs show also high trend values but only for some of the bearings. HIs derived from the frequency-domain

(DomF, SpC, SpE, SpF, SpRO) perform worse compared to HIs from the time-domain. The preprocessing steps of enveloping the signal or calculating the residual signal do not affect the HI trend behavior significantly, which can be seen in Tables A1–A3. The TDI-, and DWTRMS-HI for specific frequency bands also show high average values with changing variance (see Table A4). If these HIs would be used for robot gear condition monitoring, the progress of all frequency band specific HIs would have to be tracked as different faults stimulate changes in different frequency bands.
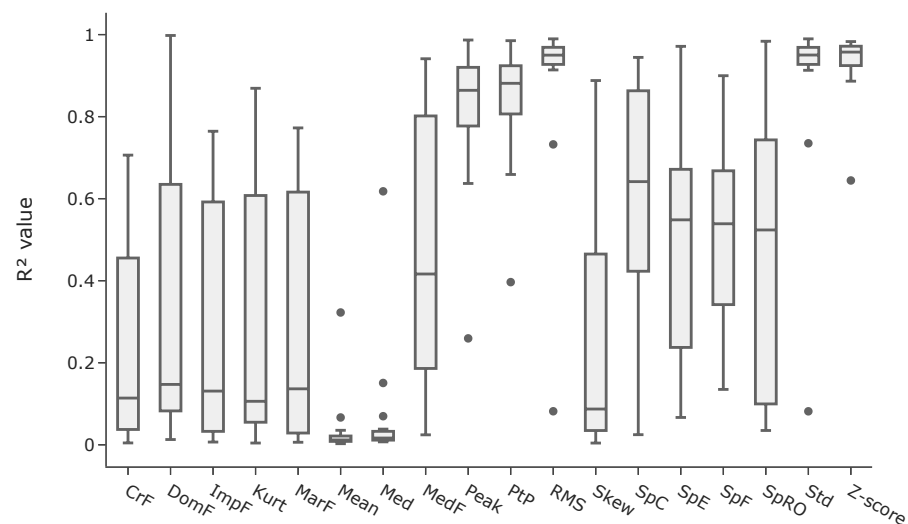
Figure 8. R^2 values for different HIs and bearings from the FEMTO data set based on raw signals.

3.2. Temperature Sensitivity Analysis

Based on this result, we conducted the temperature sensitivity analysis for the PtP-, Peak-, RMS-, Std-, TDI-, DWTRMS- and Z-score-HI. Here, we used one measurement per temperature step as the reference quantity for the Z-score-HI and set R to 128. Figure 9 shows the change of the HIs per axis in percent for the PtP-, Peak-, RMS-, Std- and Z-score-HI. The RMS- and Z-score-HI show the lowest temperature sensitivity overall. Figure 10 shows the results for the DWTRMS-HIs. Here, high sensitivities for different detail coefficient DWTRMS-HIs exist. Figure A1 shows the temperature sensitivity of the TDI-HIs of different frequency bands. Here, a similar result can be seen compared to the DWTRMS-HIs. The data of Figures 10 and A1 can also be found in Tables A5 and A6. In general, the data from axis 4 show the highest temperature sensitivity for all HIs. The comparably higher sensitivity of the HI values derived from data at axis 4 can be related to the robot trajectory. During the trajectory, the robot arm was stretched out, which leads to greater elasticity at the position of the sensor at axis 4. This can cause increased vibrations, which are magnified under changing temperature influences. Given the results of the temperature sensitivity analysis, we analyzed the data sets from the accelerated wear tests with only the RMS- and the Z-score-HI. The other HIs were excluded due to their high temperature sensitivity. Even though some frequency band specific DWTRMS-HIs and TDI-HIs show low sensitivity, they were excluded as robot gear faults do not have to stimulate these frequency bands with low sensitivity.
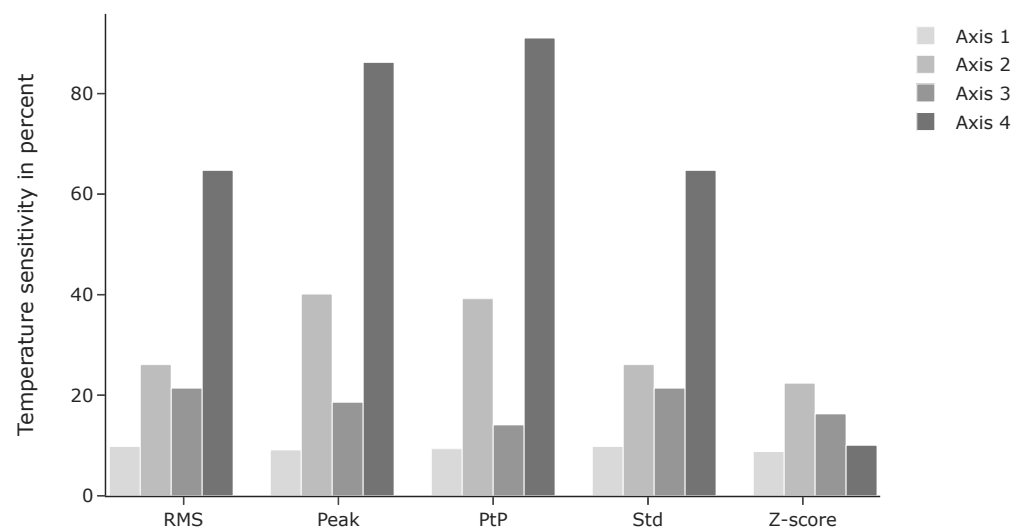
Figure 9. Temperature sensitivity for different HIs and robot axes.
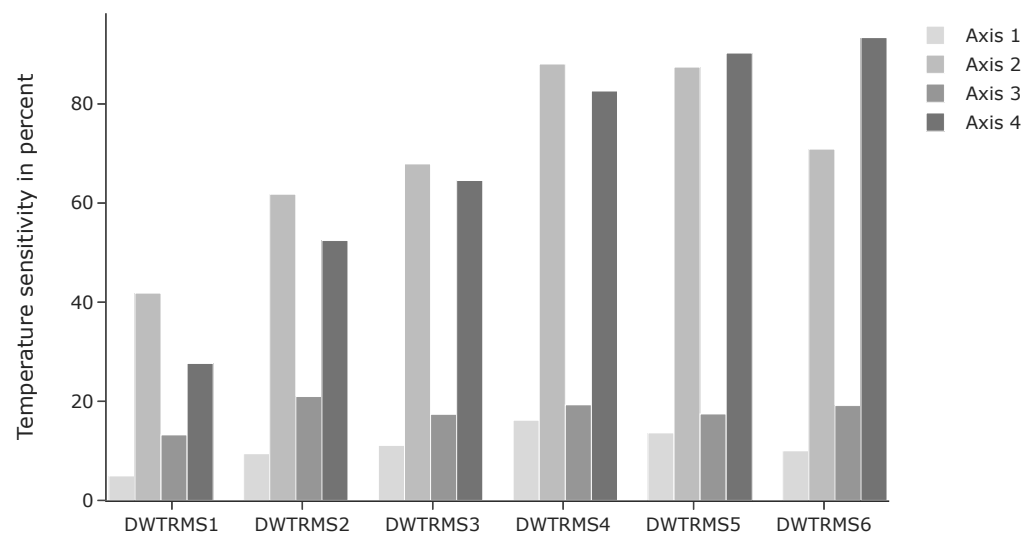
Figure 10. Temperature sensitivity for different DWTRMS-HIs and robot axes.

3.3. Accelerated Wear Tests Analysis

In this analysis, we used the first 100 measurements as the reference quantity for the Z-score-HI and set R to 256. For smoothing, we applied a rolling average with a window length of 15 on both HI series. The progress of the HIs in the accelerated wear test of the ABB IRB 7600 is shown in Figure 11. Both HIs show a plateau with increased values at the end of the experiment. It can be assumed that, at this point in time, faults have already been present. Here, the increased HI values over a longer time period could have been used as a decision criterion for maintenance actions.
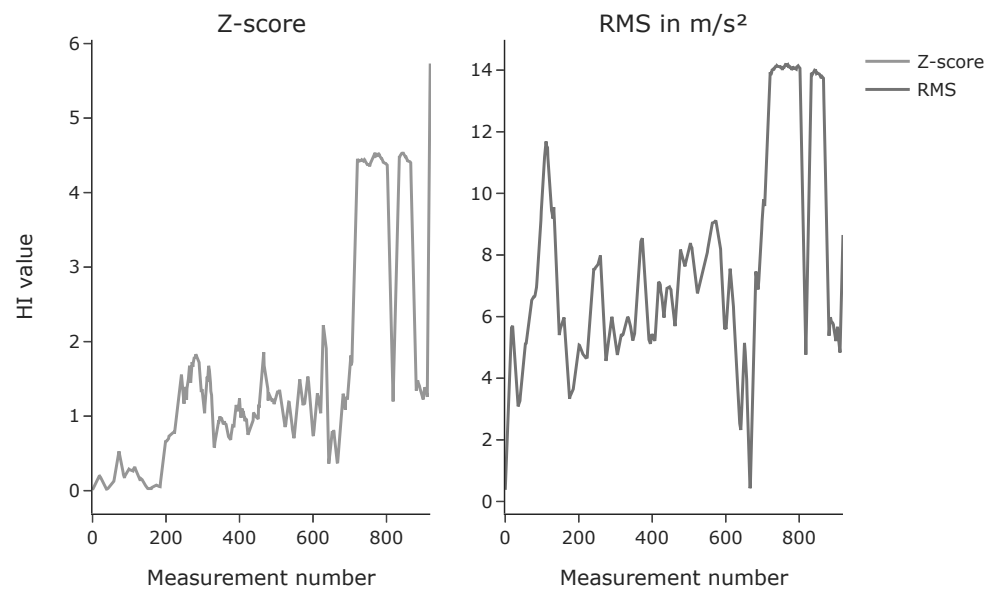
Figure 11. Z-score-HI and RMS-HI for the IRB 7600 experiment.

The measurements at the very end show decreased values again. We assume that this decrease is correlated to a part of the bearing roller. In the end of the experiment, one of the roller elements showed a large pit. During the measurements showing the higher HI values this detached part of the roller element could have been still slightly fixed at the roller element and thus could have caused high vibration. After full detachment, this noise level decreased again. For the measurements before the plateau, the RMS-HI shows higher fluctuations compared to the Z-score-HI. For instance, the RMS-HI shows a first high peak around measurement 100. Such peaks could lead to false alarms in a condition monitoring scenario and should be avoided.

The progress of the HIs in the other accelerated wear test performed with the ABB IRB 6600 is shown in Figure 12. Here, the Z-score-HI shows a trending behavior and the RMS shows a stationary progress. Both HIs show a high increase during the last measurements. In this experiment, the trending behavior of the Z-score could have been a criterion to execute maintenance actions. This information is not present in the RMS-progress. Based on the fact that the Z-score showed a better trend behavior in the ABB IRB 6600 experiment and less noisy behavior in the ABB IRB 7600 experiment, we suggest the use of the Z-score-HI for the condition monitoring of robot gears.
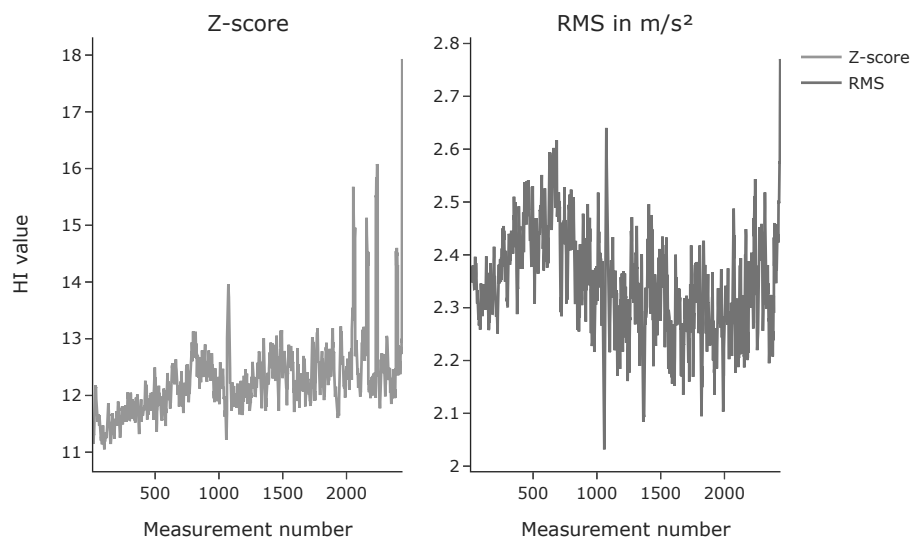
Figure 12. Z-score-HI and RMS-HI for the IRB 6600 experiment.

## 4. Discussion

The discussion is divided in four parts. First, some remarks regarding our designed HI are given. Afterwards, three parts make up the Results subsections.

To derive the spectrograms required for the Z-score-HI, the length of the window function must be defined. High values for *R* result in a high frequency resolution and low values in a high time resolution. For the individual experiments, we chose window lengths that lead to a good compromise between time and frequency resolution by inspecting spectrograms created with different window lengths. We chose window lengths that lead to spectrograms appearing the least noisy in a visual inspection. In an industrial setting, an automated approach should be developed for this dependent on the robot's trajectory and the used sensor.

The motivation to use the FEMTO data set to investigate HI performance was to assess HIs' capability to detect multiple faults. Within a robot gearbox, which are mostly RV reducers, not only bearings but also the gear teeth can have faults. Such faults are not taken into account by our analysis explicitly. However, the bearing faults present in the FEMTO data set, e.g., pitting, are similar to typical gear teeth or shaft damage from a signal analysis point of view. Damage from all components modulate the acceleration signals at a specific frequency and its sidebands. Exactly this capability to track such changes in the signal was investigated in our analysis. There also exist HIs that track energy changes at the specific component fault frequencies. Such HIs were excluded from our analysis because expert knowledge about the geometric characteristics of the gears, e.g., the bearing diameters or the number of roller elements, is required to calculate these HIs. This expert knowledge is usually not available to industrial robot users. We also excluded HIs that could be derived automatically from machine learning models, such as autoencoders, as the physical interpretation of these HIs is difficult and hence a transferability between different robot systems is questionable from our point of view.

Regarding the results of the temperature sensitivity analysis, it must be pointed out that the results are valid only for the chosen robot trajectory. As the dynamic behavior of the robot changes within its working space, this analysis should be performed individually for trajectories and robot systems. However, from a theoretical point of view, the Z-score-HI possesses the ability to cope with these temperature fluctuations independently of the trajectory. Temperature variations lead to variance in the STFT spectrograms. This variance is taken into account in the $spec(\tau, \omega)_{avg,ref}$ and $spec(\tau, \omega)_{std,ref}$ during the initialization phase. Hence, Z-score-HIs derived from measurements from functional robot gears and different temperatures will show only little differences in the Z-score-HI value. This becomes more clear considering Figure 13. Here, the STFT and Z-score spectrograms from two vibration measurements of the temperature sensitivity experiment are shown. On the left side, the spectrograms from a cold gear measurement are depicted. On the right side, the spectrograms from a warm gear measurement are shown. Differences are visible in the STFT spectrograms around seconds 1 and 2. No differences are visible in the Z-score spectrograms. The scales of the STFT spectrograms reach from -5 to 0 and the scales of the Z-score spectrograms from 0 to 1.5. Hence, the relative changes of the STFT spectrograms are bigger compared to the Z-score spectrograms. In this example, the total relative change in energy in the STFT spectrogram is 9.15 percent, whereas the total relative change in the Z-score spectrogram is just 1.63 percent.

Finally, the results from the accelerated wear tests show noisy progress over time. This hinders a simple or automated detection of faults in a condition monitoring behavior. To establish an automated CM system, a suitable trend detection in combination with an outlier detection system must be set up. A trend detection system could identify HI progress shown as in Figure 12, whereas an outlier detection system could detect progress as depicted in Figure 11. The development of such a system also marks the outlook of our future work.
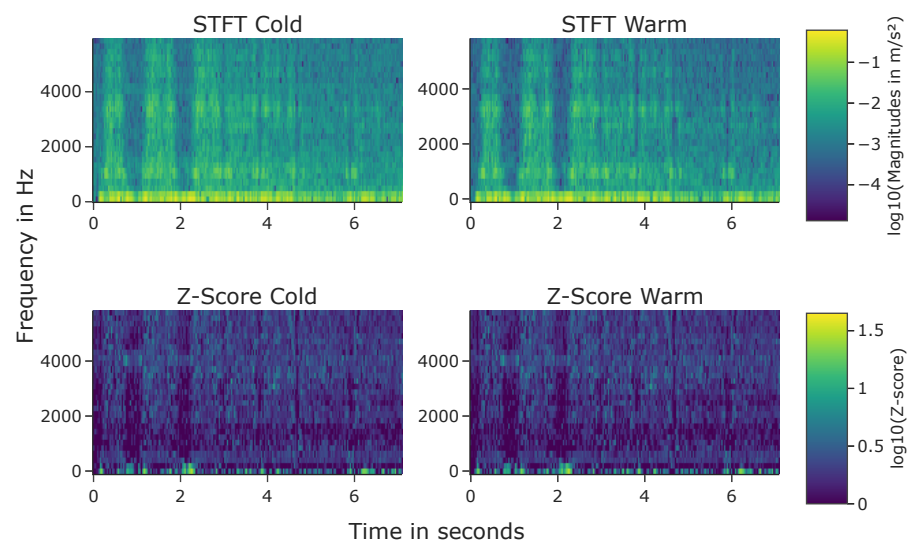
Figure 13. Spectrograms from cold and warm gear measurements.

5. Conclusions

Condition monitoring of robot gears has the potential to decrease production system downtimes. The state-of-the-art provides many health indicators to track the health state of gears. We analyzed these health indicators regarding specific requirements rising from typical industrial robot applications. These requirements are the ability to detect different faults, low temperature sensitivity and the capability to deal with instationary velocity behavior. Additionally, we suggested a new health indicator based on STFT spectrograms and Z-scores that can cope with these requirements. Our analysis showed that the RMS health indicator and our suggested health indicator meet the defined requirements the best. Data from accelerated wear tests show that for an automatic condition monitoring system a combination of a trend detection and an outlier detection system that can deal with a noisy signal is required.

Appendix A

Table A1. R^2 statistics for HIs derived from the normal signal.

	CrF	DomF	ImpF	Kurt	MarF	Mean	Med	MedF	Peak	PtP	RMS	Skew	SpC	SpE	SpF	SpRO	Std	Z-Score
Mean	0.231	0.354	0.287	0.336	0.296	0.034	0.063	0.467	0.822	0.844	0.887	0.242	0.599	0.488	0.514	0.491	0.887	0.934
Std	0.246	0.351	0.289	0.334	0.298	0.076	0.147	0.311	0.173	0.145	0.215	0.289	0.298	0.281	0.225	0.322	0.215	0.080
Min	0.005	0.013	0.007	0.004	0.006	0.003	0.007	0.024	0.259	0.397	0.082	0.004	0.025	0.067	0.135	0.035	0.082	0.644
Max	0.706	0.998	0.764	0.869	0.773	0.323	0.618	0.941	0.987	0.985	0.990	0.888	0.944	0.971	0.900	0.984	0.990	0.983

Table A2. R^2 statistics for HIs derived from the enveloped signal.

	CrF	DomF	ImpF	Kurt	MarF	Mean	Med	MedF	Peak	PtP	RMS	Skew	SpC	SpE	SpF	SpRO	Std
Mean	0.215	0.139	0.284	0.299	0.296	0.776	0.819	0.496	0.816	0.816	0.872	0.275	0.605	0.464	0.462	0.514	0.898
Std	0.229	0.248	0.283	0.328	0.291	0.296	0.248	0.318	0.178	0.178	0.227	0.303	0.286	0.298	0.276	0.309	0.131
Min	0.005	0.001	0.006	0.001	0.005	0.010	0.014	0.023	0.246	0.246	0.074	0.008	0.046	0.013	0.012	0.007	0.427
Max	0.635	0.997	0.741	0.919	0.766	0.977	0.983	0.981	0.988	0.988	0.989	0.905	0.939	0.978	0.901	0.987	0.987

Table A3. R^2 statistics for HIs derived from the residual signal as suggestet by [4].

	CrF	DomF	ImpF	Kurt	MarF	Mean	Med	MedF	Peak	PtP	RMS	Skew	SpC	SpF	SpRO	Std	SpE
Mean	0.329	0.423	0.348	0.365	0.355	0.032	0.088	0.608	0.847	0.859	0.884	0.237	0.701	0.609	0.605	0.884	0.534
Std	0.270	0.348	0.303	0.337	0.312	0.089	0.187	0.292	0.178	0.153	0.221	0.319	0.196	0.202	0.213	0.221	0.316
Min	0.010	0.021	0.003	0.007	0.018	0.001	0.001	0.016	0.211	0.328	0.082	0.003	0.425	0.147	0.132	0.083	0.023
Max	0.802	0.992	0.828	0.858	0.830	0.374	0.671	0.988	0.987	0.987	0.990	0.943	0.959	0.930	0.977	0.990	0.969

Table A4. R^2 statistics for HIs derived from the time–frequency-domain. DWT-, IMF-, and TDI-based HIs were calculated for different frequency bands. The frequency bands are encoded in the abbreviation of the HI name. Large numbers correspond to high frequency bands for TDI-HIs and low frequency bands for DWT- and IMF-HIs.

	Mean	Std	Min	Max
DWTRMS5	0.891	0.207	0.099	0.990
DWTRMS4	0.889	0.223	0.032	0.988
TDI33	0.882	0.087	0.583	0.965
DWTRMS6	0.882	0.216	0.117	0.991
TDI43	0.871	0.156	0.296	0.983
IMFRMS2	0.869	0.227	0.014	0.991
TDI36	0.867	0.203	0.095	0.976
TDI14	0.865	0.154	0.327	0.970
TDI35	0.864	0.202	0.096	0.981
TDI22	0.862	0.196	0.135	0.963
TDI34	0.861	0.197	0.114	0.974
TDI23	0.860	0.181	0.200	0.961
TDI21	0.859	0.197	0.147	0.971
DWTRMS3	0.859	0.245	0.019	0.998
TDI37	0.857	0.208	0.072	0.969
TDI39	0.853	0.221	0.017	0.975
TDI15	0.847	0.218	0.035	0.982
IMFRMS1	0.845	0.210	0.091	0.978
TDI44	0.844	0.223	0.004	0.984
TDI13	0.842	0.224	0.015	0.975
TDI12	0.841	0.218	0.022	0.969
TDI40	0.840	0.215	0.072	0.969
TDI24	0.837	0.223	0.027	0.954
TDI41	0.836	0.221	0.061	0.970
TDI16	0.833	0.228	0.022	0.969
TDI42	0.830	0.221	0.072	0.964
TDI18	0.830	0.237	0.044	0.976
TDI10	0.830	0.214	0.025	0.966
TDI5	0.827	0.273	0.032	0.995
TDI6	0.825	0.263	0.015	0.983
TDI8	0.825	0.206	0.051	0.948
TDI9	0.824	0.209	0.047	0.954
TDI4	0.823	0.273	0.151	0.995
TDI45	0.820	0.220	0.013	0.986
TDI20	0.818	0.277	0.066	0.963
TDI38	0.816	0.259	0.038	0.972
TDI32	0.815	0.272	0.090	0.968
TDI46	0.813	0.218	0.023	0.987
TDI7	0.813	0.264	0.008	0.973
TDI47	0.812	0.217	0.013	0.988
TDI11	0.812	0.251	0.017	0.966
TDI17	0.808	0.293	0.005	0.967
DWTRMS2	0.804	0.297	0.101	0.981
IMFRMS3	0.803	0.243	0.025	0.961
TDI3	0.803	0.290	0.148	0.987
TDI49	0.792	0.215	0.018	0.990
TDI19	0.782	0.304	0.026	0.959
TDI28	0.782	0.270	0.014	0.960
TDI50	0.780	0.216	0.026	0.989
TDI52	0.770	0.216	0.025	0.989
TDI30	0.769	0.293	0.049	0.964
TDI25	0.769	0.290	0.025	0.966
TDI53	0.767	0.215	0.025	0.989
TDI54	0.766	0.215	0.025	0.990

Table A4. *Cont.*

	Mean	Std	Min	Max
TDI48	0.765	0.252	0.024	0.988
TDI55	0.765	0.215	0.028	0.989
TDI58	0.762	0.215	0.026	0.990
TDI57	0.761	0.216	0.028	0.989
TDI60	0.756	0.222	0.028	0.989
TDI31	0.747	0.312	0.073	0.971
TDI51	0.747	0.253	0.022	0.989
TDI29	0.744	0.297	0.032	0.961
TDI2	0.744	0.319	0.069	0.977
DWTRMS1	0.740	0.306	0.026	0.978
TDI27	0.739	0.292	0.027	0.954
TDI63	0.736	0.253	0.028	0.989
TDI62	0.736	0.254	0.026	0.990
TDI59	0.735	0.254	0.024	0.990
TDI56	0.735	0.254	0.023	0.989
TDI61	0.734	0.254	0.024	0.989
TDI64	0.732	0.254	0.024	0.989
TDI26	0.712	0.342	0.043	0.964
IMFRMS4	0.665	0.335	0.035	0.985
HHTentr	0.646	0.317	0.021	0.982
TDI1	0.588	0.313	0.011	0.937
IMFRMS5	0.567	0.313	0.016	0.934
IMFRMS6	0.460	0.223	0.110	0.829
DecompRate	0.458	0.292	0.075	0.974
DWTKurt5	0.383	0.296	0.014	0.821
DWTKurt2	0.381	0.318	0.007	0.815
DWTEntr6	0.380	0.319	0.017	0.991
DWTImpF2	0.377	0.308	0.005	0.806
DWTKurt4	0.361	0.315	0.007	0.851
DWTKurt6	0.353	0.330	0.003	0.860
DWTImpF6	0.327	0.280	0.001	0.796
DWTImpF5	0.326	0.274	0.001	0.766
IMFRMS7	0.326	0.271	0.026	0.863
TDI0	0.325	0.246	0.037	0.906
DWTImpF3	0.325	0.260	0.017	0.701
IMFKurt1	0.320	0.314	0.009	0.816
DWTKurt3	0.319	0.296	0.007	0.827
DWTImpF4	0.302	0.273	0.004	0.748
IMFImpF1	0.288	0.280	0.009	0.838
IMFKurt3	0.287	0.288	0.017	0.843
IMFKurt4	0.286	0.222	0.024	0.677
DWTKurt1	0.282	0.217	0.012	0.722
IMFImpF4	0.277	0.202	0.014	0.601
IMFKurt2	0.263	0.274	0.010	0.689
IMFEntr2	0.254	0.265	0.012	0.867
DWTEntr5	0.254	0.291	0.001	0.989
DWTImpF1	0.251	0.213	0.006	0.660
IMFImpF3	0.242	0.253	0.016	0.761
IMFEntr1	0.232	0.280	0.009	0.944
IMFImpF2	0.224	0.185	0.011	0.602
IMFEntr3	0.207	0.269	0.013	0.888
IMFKurt5	0.184	0.215	0.007	0.822
IMFRMS8	0.181	0.238	0.000	0.682
IMFImpF5	0.164	0.187	0.007	0.693
IMFEntr4	0.153	0.138	0.005	0.524
DWTEntr4	0.136	0.235	0.005	0.969
IMFImpF6	0.121	0.118	0.010	0.377
IMFKurt6	0.121	0.125	0.010	0.428

Table A4. *Cont.*

	Mean	Std	Min	Max
IMFEntr6	0.105	0.102	0.009	0.393
DWTEntr3	0.101	0.187	0.003	0.783
IMFEntr5	0.095	0.095	0.002	0.367
IMFEntr7	0.089	0.092	0.003	0.276
DWTEntr2	0.062	0.111	0.001	0.417
IMFImpF7	0.048	0.039	0.002	0.134
IMFKurt7	0.042	0.033	0.002	0.106
IMFEntr8	0.032	0.111	0.000	0.461
DWTEntr1	0.031	0.034	0.003	0.141
IMFImpF8	0.026	0.028	0.000	0.078
IMFKurt8	0.021	0.031	0.000	0.114
IMFRMS9	0.000	0.000	0.000	0.000
IMFKurt9	0.000	0.000	0.000	0.000
IMFImpF9	0.000	0.000	0.000	0.000
IMFEntr9	0.000	0.000	0.000	0.000
IMFRMS10	0.000	0.000	0.000	0.000
IMFImpF10	0.000	0.000	0.000	0.000
IMFKurt10	0.000	0.000	0.000	0.000
IMFEntr10	0.000	0.000	0.000	0.000
IMFRMS11	0.000	NaN	0.000	0.000
IMFImpF11	0.000	NaN	0.000	0.000
IMFKurt11	0.000	NaN	0.000	0.000
IMFEntr11	0.000	NaN	0.000	0.000

Table A5. Temperature sensitivity of the different DWTRMS-HIs.

	1	2	3	4
DWTRMS1	4.944734	41.833250	13.225817	27.640727
DWTRMS2	9.431779	61.784386	20.966405	52.444752
DWTRMS3	11.100870	67.906341	17.372290	64.555873
DWTRMS4	16.176322	88.064015	19.294715	82.614996
DWTRMS5	13.631686	87.439763	17.451681	90.271799
DWTRMS6	10.015797	70.887870	19.141733	93.391435

Table A6. Temperature sensitivity of the different TDI-HIs.

	Axis 1	Axis 2	Axis 3	Axis 4
TDI0	7.887680	3.623626	4.032428	9.856386
TDI1	7.345230	13.780192	1.419329	15.104011
TDI2	5.702217	46.387687	23.876372	24.639909
TDI3	6.721355	47.590460	22.691756	42.390072
TDI4	10.873829	59.621503	24.158641	38.671919
TDI5	13.127752	74.783219	17.398075	54.988992
TDI6	14.670516	59.576255	12.953424	75.739203
TDI7	18.161779	57.596831	17.545132	65.254182
TDI8	15.090433	70.501830	11.004508	68.946535
TDI9	19.130819	94.756567	10.267873	63.083458
TDI10	19.817337	140.434648	22.212611	48.494003
TDI11	31.037879	152.473705	28.134321	75.366125
TDI12	33.675873	93.057559	18.953184	98.385403
TDI13	26.250892	79.866002	17.152706	92.669107
TDI14	11.635896	58.286933	24.510069	86.809206
TDI15	23.377379	46.907903	16.496553	72.502066
TDI16	30.064213	55.243855	11.119799	59.119520
TDI17	21.268743	64.332588	7.938803	79.776374

Table A6. *Cont.*

|	Axis 1	Axis 2	Axis 3	Axis 4
TDI18	9.808639	52.933143	4.197856	87.106639
TDI19	3.420408	57.102301	3.507140	94.175140
TDI20	0.062629	58.697728	5.538016	107.584154
TDI21	17.433815	60.093605	12.872000	112.916761
TDI22	23.980438	65.038102	9.486835	164.461250
TDI23	23.749318	91.055389	11.379480	152.353906
TDI24	11.483126	109.842746	21.619409	121.442989
TDI25	6.596706	85.653753	23.250270	111.067700
TDI26	16.057350	68.794132	20.724566	88.922105
TDI27	16.557670	68.373539	18.973086	114.047417
TDI28	19.372075	65.937430	13.256130	140.639806
TDI29	22.613427	68.081118	27.002980	129.175849
TDI30	15.441241	68.255349	31.219217	111.829705
TDI31	4.729546	68.353458	28.824115	116.071704
TDI32	1.112630	69.440683	18.666493	104.393062
TDI33	3.010018	66.107354	13.594603	104.544706
TDI34	6.223136	49.771212	14.597765	135.411471
TDI35	10.119042	33.536590	4.257545	167.094574
TDI36	0.777079	33.963467	0.393118	158.518025
TDI37	0.893584	47.211867	18.367647	110.996278
TDI38	8.789406	39.550853	33.938136	55.254421
TDI39	18.286551	4.903817	23.615781	35.301715
TDI40	28.767525	34.224059	6.485524	47.061077
TDI41	21.670495	39.728416	9.696093	33.227046
TDI42	4.437817	59.765908	18.549288	79.919517
TDI43	0.147523	52.939389	19.848252	83.294446
TDI44	0.446057	53.539446	19.351326	79.595920
TDI45	0.657082	52.356513	19.032092	77.824663
TDI46	0.199947	55.873800	19.528656	75.827413
TDI47	1.388775	57.010168	19.014225	76.394986
TDI48	2.097117	57.774286	18.889822	76.077127
TDI49	3.164926	58.959065	18.696796	75.814731
TDI50	3.851514	59.592621	18.410404	75.719379
TDI51	4.577587	60.339446	18.308180	75.543086
TDI52	5.160258	60.877095	18.211340	75.458546
TDI53	5.659315	61.365144	18.069126	75.348426
TDI54	6.077128	61.761218	17.976632	75.218693
TDI55	6.436426	62.077612	17.945549	75.121278
TDI56	6.763257	62.361230	17.851473	75.050770
TDI57	7.080730	62.591447	17.781367	74.975471
TDI58	7.369667	62.781646	17.783673	74.880725
TDI59	7.622924	62.946830	17.710259	74.853578
TDI60	7.828532	63.078384	17.670637	74.815067
TDI61	7.974544	63.177746	17.693925	74.733074
TDI62	8.072173	63.259698	17.636933	74.758740
TDI63	8.128858	63.308959	17.623715	74.750804
TDI64	8.147158	63.322210	17.664456	74.689287
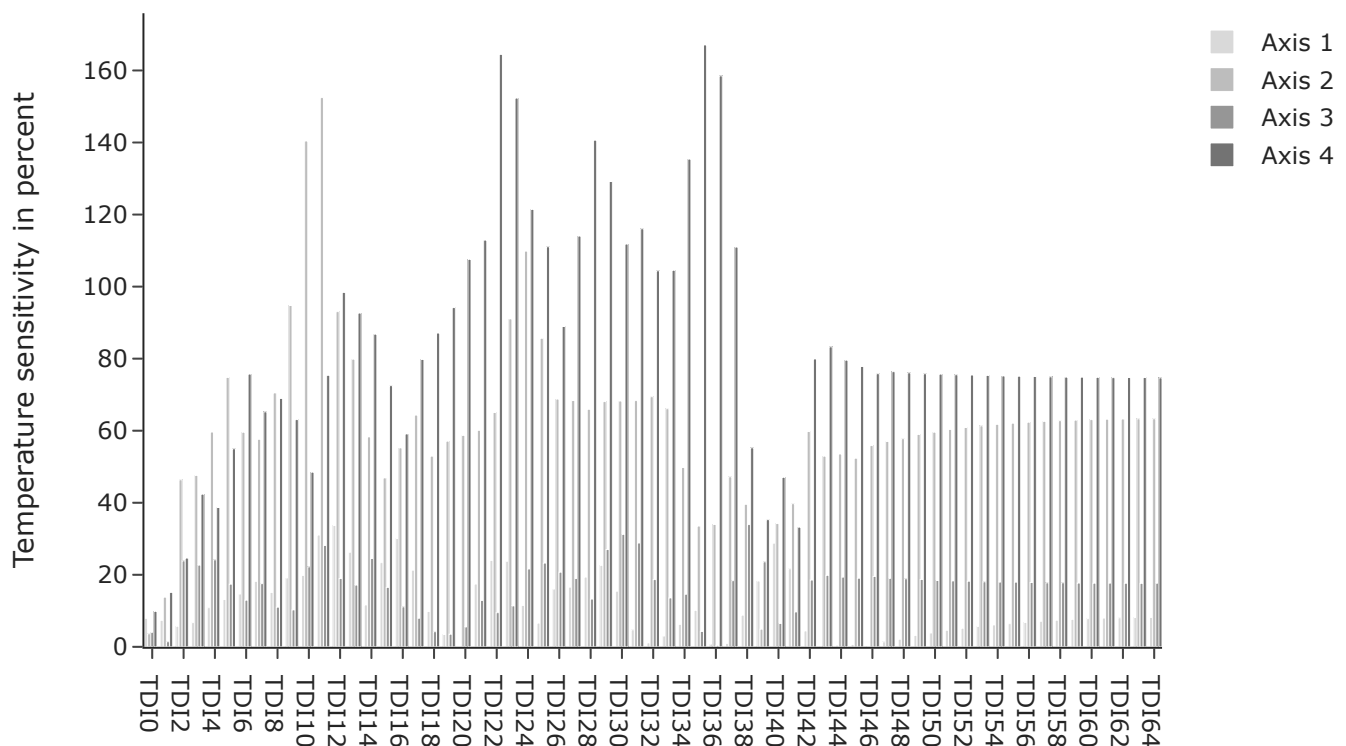
Figure A1. Temperature sensitivity for the different TDI-HIs and robot axes.

References

1. Krockenberger, O. Industrial Robots for the Automotive Industry. *Sae Tech. Pap. Ser.* **1996**. [CrossRef]
2. Lee, J.; Wu, F.; Zhao, W.; Ghaffari, M.; Liao, L.; Siegel, D. Prognostics and health management design for rotary machinery systems—Reviews, methodology and applications. *Mech. Syst. Signal Process.* **2014**, *42*, 314–334. [CrossRef]
3. ISO. *DIN ISO 17359:2018-05, Zustandsüberwachung und -Diagnostik von Maschinen—Allgemeine Anleitungen (ISO_17359:2018)*; Beuth Verlag GmbH: Berlin, Germany, 2018. [CrossRef]
4. Kim, Y.; Park, J.; Na, K.; Yuan, H.; Youn, B.D.; Kang, C.S. Phase-based time domain averaging (PTDA) for fault detection of a gearbox in an industrial robot using vibration signals. *Mech. Syst. Signal Process.* **2020**, *138*, 106544. [CrossRef]
5. Jaber, A.A. *Design of an Intelligent Embedded System for Condition Monitoring of an Industrial Robot*; Springer Theses, Recognizing Outstanding Ph.D. Research; Springer International Publishing: Cham, Switzerland, 2017. [CrossRef]
6. Zhi, H.; Yangi-Shang . Remote performance evaluation, life prediction and fault diagnosis of RV reducer for industrial robot. *J. Physics: Conf. Ser.* **2020**, *1676*, 012212. [CrossRef]
7. Hugo, D.; Benjamin, S. Robot Condition Monitoring: A first Step in Condition Monitoring for Robotic Applications. Master's Thesis, Lulea University of Technology, Lulea, Sweden, 2017.
8. Karlsson, M.; Hörnqvist, F. Robot Condition Monitoring and Production Simulation. Master's Thesis, Lulea University of Technology, Lulea, Sweden, 2018.
9. Liu, X.; Wu, X.; Liu, C.; Liu, T. Research on condition monitoring of speed reducer of industrial robot with acoustic emission. *Trans. Can. Soc. Mech. Eng.* **2016**, *40*, 1041–1049. [CrossRef]
10. Sun, H.; Zhang, J. Health Monitoring of Strain Wave Gear on Industrial Robots. In Proceedings of the 2019 IEEE 8th Data Driven Control and Learning Systems Conference (DDCLS), Dali, China, 24–27 May 2019.
11. Nentwich, C.; Junker, S.; Reinhart, G. Data-driven Models for Fault Classification and Prediction of Industrial Robots. *Procedia CIRP* **2020**, *93*, 1055–1060. [CrossRef]
12. Jahagirdar, A.C.; Gupta, K.K. Cumulative Distribution Sharpness Profiling Based Bearing Fault Diagnosis Framework Under Variable Speed Conditions. *IEEE Sensors J.* **2021**. [CrossRef]
13. Attoui, I.; Boutasseta, N.; Fergani, N. Novel Machinery Monitoring Strategy Based on Time–Frequency Domain Similarity Measurement With Limited Labeled Data. *IEEE Trans. Instrum. Meas.* **2021**, *70*, 1–8. [CrossRef]
14. Cocconcelli, M.; Zimroz, R.; Rubini, R.; Bartelmus, W. STFT Based Approach for Ball Bearing Fault Detection in a Varying Speed Motor. In *Condition Monitoring of Machinery in Non-Stationary Operations*; Fakhfakh, T., Bartelmus, W., Chaari, F., Zimroz, R., Haddar, M., Eds.; Springer: Berlin/Heidelberg, Germany, 2012; Volume 34, pp. 41–50. [CrossRef]
15. Gao, H.; Liang, L.; Chen, X.; Xu, G. Feature extraction and recognition for rolling element bearing fault utilizing short-time Fourier transform and non-negative matrix factorization. *Chin. J. Mech. Eng.* **2015**, *28*, 96–105. [CrossRef]

16. Jian, B.L.; Su, X.Y.; Yau, H.T. Bearing Fault Diagnosis Based on Chaotic Dynamic Errors in Key Components. *IEEE Access* **2021**, *9*, 53509–53517. [CrossRef]
17. Vippala, S.R.; Bhat, S.; Reddy, A.A. Condition Monitoring of BLDC Motor Using Short Time Fourier Transform. In Proceedings of the 2021 IEEE Second International Conference on Control, Measurement and Instrumentation (CMI), Kolkata, India, 8–10 January 2021, pp. 110–115. [CrossRef]
18. Veerendra, A.S.; Mohamed, M.R.; Punya Sekhar, C. A novel fault—Detection methodology of proposed reduced switch MLI fed induction motor drive using discrete wavelet transforms. *Int. Trans. Electr. Energy Syst.* **2021**, *31*. [CrossRef]
19. Defdaf, M.; Berrabah, F.; Chebabhi, A.; Cherif, B.D.E. A new transform discrete wavelet technique based on artificial neural network for induction motor broken rotor bar faults diagnosis. *Int. Trans. Electr. Energy Syst.* **2021**, *31*. [CrossRef]
20. Zhu, H.; He, Z.; Wei, J.; Wang, J.; Zhou, H. Bearing Fault Feature Extraction and Fault Diagnosis Method Based on Feature Fusion. *Sensors* **2021**, *21*, 2524. [CrossRef]
21. Kotsanidis, K.; Benardos, P. Rolling element bearings fault classification based on feature extraction from acceleration data and artificial neural networks. *Iop Conf. Ser. Mater. Sci. Eng.* **2021**, *1037*, 012008. [CrossRef]
22. Skariah, A.; Pradeep, R.; Rejith, R.; Bijudas, C.R. Health monitoring of rolling element bearings using improved wavelet cross spectrum technique and support vector machines. *Tribol. Int.* **2021**, *154*, 106650. [CrossRef]
23. Sharma, S.; Tiwari, S.K.; Singh, S. Integrated approach based on flexible analytical wavelet transform and permutation entropy for fault detection in rotary machines. *Measurement* **2021**, *169*, 108389. [CrossRef]
24. Elasha, F.; Li, X.; Mba, D.; Ogundare, A.; Ojolo, S. A Novel Condition Indicator for Bearing Fault Detection Within Helicopter Transmission. *J. Vib. Eng. Technol.* **2021**, *9*, 215–224. [CrossRef]
25. Mohanraj, T.; Yerchuru, J.; Krishnan, H.; Nithin Aravind, R.S.; Yameni, R. Development of tool condition monitoring system in end milling process using wavelet features and Hoelder's exponent with machine learning algorithms. *Measurement* **2021**, *173*, 108671. [CrossRef]
26. Duan, J.; Duan, J.; Zhou, H.; Zhan, X.; Li, T.; Shi, T. Multi-frequency-band deep CNN model for tool wear prediction. *Meas. Sci. Technol.* **2021**, *32*, 065009. [CrossRef]
27. Gómez, M.J.; Marklund, P.; Strombergsson, D.; Castejón, C.; García-Prada, J.C. Analysis of Vibration Signals of Drivetrain Failures in Wind Turbines for Condition Monitoring. *Exp. Tech.* **2021**, *45*, 1–12. [CrossRef]
28. Suresh, S.; Naidu, V.P.S. Gearbox Health Condition Monitoring Using DWT Features. In Proceedings of the 6th National Symposium on Rotor Dynamics, Bangalore, India, 2–3 July 2019; Rao, J.S., Arun Kumar, V., Jana, S., Eds.; Springer: Singapore, 2021; Volume 329, pp. 361–374.
29. de Sena, A.P.C.; de Freitas, I.S.; Filho, A.C.L.; Sobrinho, C.A.N. Fuzzy diagnostics for gearbox failures based on induction motor current and wavelet entropy. *J. Braz. Soc. Mech. Sci. Eng.* **2021**, *43*. [CrossRef]
30. Yu, D.; Yang, Y.; Cheng, J. Application of time—Frequency entropy method based on Hilbert-Huang transform to gear fault diagnosis. *Measurement* **2007**, *40*, 823–830. [CrossRef]
31. Mao, W.; He, J.; Zuo, M.J. Predicting Remaining Useful Life of Rolling Bearings Based on Deep Feature Representation and Transfer Learning. *IEEE Trans. Instrum. Meas.* **2020**, *69*, 1594–1608. [CrossRef]
32. Cheng, C.; Ma, G.; Zhang, Y.; Sun, M.; Teng, F.; Ding, H.; Yuan, Y. A Deep Learning-Based Remaining Useful Life Prediction Approach for Bearings. *IEEE/ASME Trans. Mechatron.* **2020**, *25*, 1243–1254. [CrossRef]
33. Thakker, H.T.; Dave, V.; Vakharia, V.; Singh, S. Fault Diagnosis of Ball Bearing Using Hilbert Huang Transform and LASSO Feature Ranking Technique. *Iop Conf. Ser. Mater. Sci. Eng.* **2020**, *841*, 012006. [CrossRef]
34. Larsen, R.J.; Marx, M.L. *An Introduction to Mathematical Statistics and Its Applications*, 3rd ed.; Prentice Hall: Upper Saddle River, NJ, USA, 2001.
35. Nectoux, P.; Gouriveau, R.; Medjaher, K.; Ramasso, E.; Chebel-Morello, B.; Zerhouni, N.; Varnier, C. PRONOSTIA: An experimental platform for bearings accelerated degradation tests. In Proceedings of the IEEE International Conference on Prognostics and Health Management, PHM'12, Denver, CO, USA, 23–27 September 2012.
36. Nectoux, P.; Gouriveau, R.; Medjaher, K.; Ramasso, E.; Chebel-Morello, B.; Zerhouni, N.; Varnier, C. PHM IEEE 2012 Data Challenge Data Set. Available online: https://github.com/wkzs111/phm-ieee-2012-data-challenge-dataset (accessed on 19 May 2021).
37. Arun, P.; Lincon, S.A.; Prabhakaran, N. Detection and Characterization of Bearing Faults from the Frequency Domain Features of Vibration. *IETE J. Res.* **2018**, *64*, 634–647. [CrossRef]
38. Caesarendra, W.; Tjahjowidodo, T. A Review of Feature Extraction Methods in Vibration-Based Condition Monitoring and Its Application for Degradation Trend Estimation of Low-Speed Slew Bearing. *Machines* **2017**, *5*, 21. [CrossRef]
39. Vecer, P.; Kreidl, M.; Smid, R. Condition Indicators for Gearbox Condition Monitoring Systems. *Acta Polytech.* **2005**, *45*, 35–42. [CrossRef]
40. Zhu, J.; Nostrand, T.; Spiegel, C.; Morton, B. Survey of condition indicators for condition monitoring systems. In Proceedings of the Annual Conference of the Prognostics and Health Management Society 2014, Fort Worth, TX, USA, 27 September–3 October 2014.
41. Geropp, B. Envelope Analysis—A Signal Analysis Technique for Early Detection and Isolation of Machine Faults. *IFAC Proc. Vol.* **1997**, *30*, 977–981. [CrossRef]
42. Lei, Y.; Li, N.; Guo, L.; Li, N.; Yan, T.; Lin, J. Machinery health prognostics: A systematic review from data acquisition to RUL prediction. *Mech. Syst. Signal Process.* **2018**, *104*, 799–834. [CrossRef]